



UNIVERSITY OF LEEDS

This is a repository copy of *Heat transfer enhancement in a micro-channel cooling system using cylindrical vortex generators.*

White Rose Research Online URL for this paper:
<http://eprints.whiterose.ac.uk/96797/>

Version: Accepted Version

Article:

Al-Asadi, MT, Alkasmoul, FS and Wilson, MCT (2016) Heat transfer enhancement in a micro-channel cooling system using cylindrical vortex generators. *International Communications in Heat and Mass Transfer*, 74. pp. 40-47. ISSN 0735-1933

<https://doi.org/10.1016/j.icheatmasstransfer.2016.03.002>

© 2016. This manuscript version is made available under the CC-BY-NC-ND 4.0 license
<http://creativecommons.org/licenses/by-nc-nd/4.0/>

Reuse

Unless indicated otherwise, fulltext items are protected by copyright with all rights reserved. The copyright exception in section 29 of the Copyright, Designs and Patents Act 1988 allows the making of a single copy solely for the purpose of non-commercial research or private study within the limits of fair dealing. The publisher or other rights-holder may allow further reproduction and re-use of this version - refer to the White Rose Research Online record for this item. Where records identify the publisher as the copyright holder, users can verify any specific terms of use on the publisher's website.

Takedown

If you consider content in White Rose Research Online to be in breach of UK law, please notify us by emailing eprints@whiterose.ac.uk including the URL of the record and the reason for the withdrawal request.



eprints@whiterose.ac.uk
<https://eprints.whiterose.ac.uk/>

Heat transfer enhancement in a micro-channel cooling system using cylindrical vortex generators

Mushtaq. T. Al-Asadi^{a, b}, F. S. Alkasmoul^a, M. C. T. Wilson^a

^a*Institute of Thermofluids, School of Mechanical Engineering, University of Leeds, UK*

^b*Refrigeration Department, Eng. Division, South Oil Company, Ministry of Oil, Basrah, Iraq.*

Abstract

Three-dimensional conjugate heat transfer under laminar flow conditions within a micro-channel is analysed numerically to explore the impact of a new design of vortex generator positioned at intervals along the base of the channel. The vortex generators are cylindrical with quarter-circle and half-circle cross sections, with variants spanning the whole width of the channel or parts of the channel. Micro-channels with Reynolds number ranging from 100 to 2300 are subjected to a uniform heat flux relevant to microelectronics cooling. To ensure the accuracy of the results, validations against previous microchannel studies were conducted and found to be in good agreement, before the new vortex generators with radii up to 400 μm were analysed. Using a thermal-hydraulic performance parameter expressed in a new way, the VGs described here are shown to offer significant potential in combatting the challenges of heat transfer in the technological drive toward lower weight/smaller volume electrical and electronic devices.

Keywords: vortex generators, micro-channel, hydraulic thermal performance, micro scale cooling system, heat transfer enhancement.

*Corresponding author:

Email: ml13mtka@leeds.ac.uk; M.Wilson@leeds.ac.uk

Nomenclatures

A_s	surface area of the whole heat sink (μm^2)
CFD	Computational Fluid Dynamic
C_p	Specific heat, J/kg.K
D	Diameter, μm
FEM	Finite Element Method
FVM	Finite Element Method
K	Thermal conductivity, W/m.K
L	Channel length, μm
VGs	Vortex generators
P	Pressure, N/m ²
q	Uniform heat flux, W/cm ²

Re	Reynolds number
T	Temperature, K
X	Axial distance, μm

Greek Symbols

μ	Viscosity, kg/ms
Θ	Thermal resistance
ρ	Densities, kg/m ³

Sub script

<i>ave</i>	average
<i>In</i>	inlet
<i>Out</i>	outlet
<i>S</i>	surface

1. Introduction

Recently, developments in electronic and electrical devices have led to the reduction in their volumes and weights, and managing the heat generated is becoming a real challenge to thermal system researchers [1]. Therefore there is a need to improve cooling systems by decreasing their size and weight to micro- and mini-scale systems, such as micro-channel heat exchangers and heat sinks [2], while simultaneously increasing the efficiency to meet this development [3]. Mini- and micro-channels are different from traditional channels, and can be classified according to their associated hydraulic diameters, D_h , [4-6] as presented in table 1.

The term 'micro-channel' first appeared in 1981 [7]. The concept had a great influence in thermal science as it decreased the hydraulic diameter and enhanced the heat transfer. In the revolution of advanced manufacturing processes, many experimental and numerical studies investigated the heat transfer and fluid flow performance of various modified geometries such as micro-channels with grooves and ribs [8-11]. The effect of vortex generators (VGs) on heat transfer and fluid flow characteristics were investigated experimentally in 1969 [12]. They can take various forms such as protrusions, wings, inclined blocks, winglets, fins, and ribs [13, 14], and have been used to enhance heat transfer in different geometries such as circular and non-circular ducts under turbulent flow [15-17]. They have also been used in laminar flow [18], with flat plate-fins in rectangular channels [19-21], tube heat exchangers [22], heat sinks [18, 23] and rectangular narrow channels [24, 25].

The rectangular micro-channel was the best geometry based on the numerical investigation of Xia et al. [26], who considered various microchannel shapes. They also investigated the distribution of flow through a collection of 30 microchannels forming a heat sink, considering different header chamber shapes and inlet/outlet positions.

Ebrahimi et al. [13] used finite volume based numerical analysis to study the impact of using vortex generators (VGs) with various orientations on laminar fluid flow and heat transfer regimes in a micro-channel. The results showed that the Nusselt number rose from 2-25% when the Reynolds number ranged from 100 to 1100, whilst the maximum increase of friction factor was 30% when using the VGs. Various other recent investigations have also indicated potential benefits of using VGs with laminar flow at different Reynolds number [24, 27, 28]. However, there remains a need for deeper understanding of VG performance over a wider range of laminar flow, for example to minimize the pressure drop penalty resulting from the introduction of VGs.

A 2D numerical study utilized smooth channel with fixed heat flux applied to the wall sides having an adiabatic cylinder inside which was perpendicular to the laminar flow direction with Reynolds number of 100 and Prandtl number ranging from 0.1 to 1 [3]. The authors have investigated the influence of the distance between the base and the top of the channel as they

found that the maximum enhancement when the cylinder was fixed in the half way from the base. Also the results showed that the low Prandtl number affective positively on heat transfer enhancement.

Furthermore, a modified channel having cylindrical vortex generators inside a uniform channel using turbulent flow with Reynolds number of 3745 has been investigated numerically [29]. It was found that utilizing a cylindrical vortex generator enhanced the heat transfer by 1.18 times compared to the uniform channel.

Based on the published literature and the Author's knowledge there is no study done to investigate the influence of the diameter of half cylindrical vortex generators placed along the base of the channel' at the end of the final sentence.

This study therefore proposes and explores new geometry designs not previously considered: specifically VGs based on cylinders with half-circular and quarter-circular cross-sections are introduced into rectangular micro-channel heat sinks. Several lateral variations of these VGs are also considered, namely full-span cylinders, shorter centred cylinders, and split/separated cylinders. The optimal radii of the VGs are also established. Section 2 describes the geometry in more detail, after which Section 3 discusses the mathematical model and Section 4 the numerical approach and validation process. The main results are discussed in Section 5, and conclusions are drawn in Section 6.

2. Geometry description

The base geometry considered is a single micro-channel with rectangular cross-section, as shown in Fig. 1(a). Such channels are common in the heat sinks designed for CPUs (Fig. 1b), where they form the gaps between the parallel fins of the heat sink, and that is the application considered here, with the base area of the heat sink taken as $A_s = 6.27 \times 10^8 \mu\text{m}^2$. Within the channel, a number of cylindrical vortex generators are equally distributed along the base. These have cross-sections that are either a quarter-circle or half-circle, as shown in Fig. 1(c) and (d) respectively, and a variable radius, r , ranging up to $400 \mu\text{m}$. The micro-channel dimensions are given in Table 2. The table also shows the three different spanwise configurations considered, namely: 'full-span', where the VG occupies the full width of the micro-channel; 'centred', where the VG is shorter than the channel width and is centred; and 'split', which is the same as the centred configuration except that the VG is split into two equal parts, with a gap of $50\text{-}100 \mu\text{m}$ between them. Table 2 includes a view of the VGs looking along the channel from the inlet.

3. Mathematical modelling

3.1. Governing equations and key parameters

The water flow in the micro-channel is considered to be laminar, steady, incompressible and Newtonian, with gravitational and viscous dissipation effects neglected. With $\mathbf{u} = (u, v, w)$ representing the liquid velocity in (x, y, z) Cartesian coordinates, and p , ρ and μ denoting the liquid pressure, density and viscosity respectively, the (dimensional) governing equations for the flow are the usual continuity and Navier-Stokes equations:

$$\nabla \cdot \mathbf{u} = 0 \quad (1)$$

$$\rho(\mathbf{u} \cdot \nabla)\mathbf{u} = -\nabla p + \mu \nabla^2 \mathbf{u}. \quad (2)$$

The energy equation for the liquid phase in the micro-channel is

$$\rho C_p \mathbf{u} \cdot \nabla T_L = k \nabla^2 T_L \quad (3)$$

where C_p , T_L , and k are respectively the specific heat, temperature, and thermal conductivity of the liquid. Conduction in the solid is captured by

$$\nabla \cdot (k_S \nabla T_S) = 0 \quad (4)$$

where T_S and k_S are respectively the temperature and thermal conductivity of the solid.

The Reynolds number is here defined in terms of the inlet velocity, u_{in} , and hydraulic diameter as

$$Re = \frac{\rho u_{in} D_h}{\mu}. \quad (5)$$

The heat transfer performance is quantified by the thermal resistance, defined as

$$\Theta = \frac{T_{ave} - T_{in}}{A_S q}, \quad (6)$$

where T_{ave} is the average temperature of the base, T_{in} is the inlet temperature, and q is the heat flux through the base of the heat sink. To give a balanced assessment of the effective heat transfer enhancement provided by VGs, taking into account the penalty paid in terms of the pressure drop, a thermal-hydraulic performance evaluation criteria (PEC) index [8, 9] is used, which in this study is defined as:

$$PEC = \frac{\Theta/\Theta_s}{(\Delta P/\Delta P_s)^{1/3}} \quad (7)$$

where ΔP and Θ are the pressure drop and thermal resistance in a microchannel containing VGs and ΔP_s and Θ_s are the same quantities in the corresponding smooth (i.e. uniform) micro-channel.

3.2 Boundary conditions

As indicated in Fig. 1(f), symmetry conditions were applied at the left- and right-hand outer boundaries of the domain, while a uniform heat flux was applied at the bottom boundary. The top boundary was considered as adiabatic. At the inlet, the velocity of the flow was set in terms of the specified Reynolds number using (5), and the inlet temperature was fixed at 293.15 K. At the outlet, the pressure was set to zero, and on the micro-channel walls the no slip condition was applied.

4. Numerical method, mesh, and code validation

Equations (1)-(4) were solved simultaneously using the finite element software COMSOL Multiphysics version 4.4. A grid independence test was applied on both smooth channel and a VG-enhanced channel to assess the density of mesh required. For the smooth channel, five meshes were used, labelled as 'coarser', 'coarse', 'normal', 'fine', and 'finer', with number of elements 53554, 145869, 283944, 788230, and 2831904 respectively, and Fig. 2 shows the maximum temperature calculated using each mesh. As can be seen, the 'fine' mesh provided the best run time while ensuring mesh independence of the solution. Therefore, the standard fine 'physics-controlled' mesh was considered. Whilst, modified fine physics-controlled meshes were applied on VGs micro-channel models. Chosen modifications of mesh (M1) were mainly in the whole size of the geometry which presented in maximum elements, minimum elements, and growth ratio 100, 10, and 1.15 respectively as they shown in Fig.3.

To ensure the accuracy of the results, two simulation models were compared with previous numerical studies. The first validation model was compared with Shkariah et al.[30], who modelled a graphene micro-channel within a heat sink using the finite volume-based software FLUENT. Figs. 4 and 5 show a comparison of the present COMSOL simulations with the published calculations, with the inlet temperature set at 300 K, the flow rate at 8.6 cm³/s, and the heat flux at two values: 181 and 277 W/cm². Good agreement is seen between the two approaches. The second validation was with Abdollahi, and Shams [31]. They investigated the impact on conjugate heat transfer of using rectangular vortex generators with various orientations and their inclination in a channel, with water as the working fluid. The validation was done with present study and showed good agreement, utilizing an angle for VG of 45^o, heat flux of 1kW/m², and values for Reynolds number of 233 and 350 as shown in Table 3.

5. Results and discussions

Some 500 three-dimensional laminar flow simulations were conducted with Reynolds number in the range 100-2300 and heat flux ranging from 100 to 300 W/cm² to assess the impact of the vortex generators described in Section 2 on the conjugate heat transfer, with water as the working fluid. As to be expected, it was found that the thermal resistance was decreased as the Reynolds number increased due to the increase of the velocity which leads to an enhanced heat transfer rate, however the price paid is an increase in pressure drop to drive the faster flow.

The results presented below focus on the particular value of 100 W/cm² for the heat flux, because this corresponds to the upper temperature limit for operation of electronic devices [17, 32-34]. Before discussing in detail the effects of the vortex generators, Fig. 6 shows a typical plot of thermal resistance and pressure drop versus Reynolds number for different heat flux values. As can be seen, the same trends are observed in each case. Increasing the heat flux results in a very slight improvement in thermal resistance and a larger improvement (i.e. reduction) in the pressure drop. This is typical of the results found, so in what follows attention will be restricted to the case of $q = 100 \text{ W/cm}^2$.

5.1. Quarter-circle VG models

Vortex generators with cross section shown in Fig. 1(c) and spanwise configuration shown in Table 2 were inserted into the microchannel and the performance was analysed over a range of radii and Reynolds numbers. The same trends were observed for the 'full-span', 'centred' and 'split' VGs (see Table 2 for definitions), so two models are considered here to present the effect of the VG radius on the conjugate heat transfer for various values of Reynolds number.

Fig. 7 shows the influence of radius ranging from 0 to 400 μm on the thermal resistance and pressure drop using full-span VGs at three relatively low Reynolds numbers. Introducing the VGs with radii $r = 100 \mu\text{m}$ and $200 \mu\text{m}$ raises the thermal resistance slightly, hence degrading performance, at all three values of Re . Increasing the radius to $300 \mu\text{m}$ then reduces the thermal resistance slightly, but it is only at $Re = 500$ that θ is reduced below its value for the uniform channel with no VGs. Interestingly, a further increase of radius to $400 \mu\text{m}$ produces another slight increase in θ at $Re = 700$ and 900 and the same performance at $Re = 500$, suggesting that there is a local minimum in θ at around $r = 300 \mu\text{m}$. In all cases, the pressure drop increases with VG radius, consistent with the increasing constriction of the flow.

Fig. 8(a) shows the impact of radius on the thermal resistance and the pressure drop at high Reynolds number ranging from 1100 to 2300 using 'split' VGs (see Table 2). Both the pressure drop and the thermal resistance increase as the radius increases. This can be attributed to

hot spots which are behind each VG because of low velocity at these areas, see example contour plots in Fig. 8(b). Hence it can be concluded that VGs with a quarter-circle cross-section are not beneficial.

5.2. Half-circle VGs

The other VG geometry considered in this work is that of cylinders with a half-circle cross-section as shown in Fig. 1(d). Again the three different spanwise configurations shown in Table 2 were considered. Fig. 9 presents the impact of the radius of full-span VGs on the thermal resistance and pressure drop for a range of Reynolds numbers, which is split into two plots for the sake of clarity. Unlike the quarter-circle VGs, for the half-circle case, the thermal resistance decreases monotonically with radius for all Reynolds numbers above 100. The thermal resistance also decreases as Re increases, but of course the pressure drop increases.

Having seen that the full-span half-circle VGs appear to offer benefits, modifications to the VGs are now considered. First, the span of the VG is reduced to 300 μm and it is positioned centrally across the gap, creating the 'centred' VG shown in Table 2, which has a gap between the VG and the side walls of the micro-channel. Fig. 10 shows θ and ΔP as a function of the VG radius for the centred VG, with the range of Reynolds number again split for clarity. Interestingly, there is a change in behaviour as the VG radius is increased above 200 μm . For the lower Re range, the rate of decrease of θ with r slows before increasing again, producing something of a 'kink' in the plot at 200 μm . For the higher Re range, there is also a noticeable change in the rate at which θ changes with r , but in contrast this involves a more significant reduction in the thermal resistance above $r = 200 \mu\text{m}$. Comparing Fig. 10 with Fig. 9, it is clear that the thermal resistance is lower for the centred VG at high Re and larger radius. This is probably because the gap between the end of the VG and side wall of the channel allows heat transfer to continue along the whole length of the side wall.

A second modification of the VG is to split the 'centred' VG in the middle, thus introducing an additional central gap as shown in the 'split' geometry row of Table 2. Fig. 11 shows the corresponding plots of thermal resistance and pressure drop against radius. In terms of thermal resistance, the introduction of the central gap negates the benefits seen with the centred VG, and the behaviour is similar to that of the full-span VG. However, the central gap does produce a reduction in the pressure drop compared to the full-span VGs under equivalent conditions.

Fig. 12 compares the thermal resistance and pressure drop observed using each of the three half-circle VG designs, along with those of the smooth, uniform channel with no VGs present. The VG radius in each case is 200 μm . It is found that the lowest thermal resistance is

achieved with the centred VG, then the split, then the full-span VGs, and all the VGs produce a lower thermal resistance than the uniform channel with no VGs present. On the other hand, all VGs resulted in higher pressure drops than the uniform channel, as is to be expected. The lowest pressure drop with VGs present is seen with the centred, then split, then full-span VGs – i.e. the same ranking as for the thermal resistance.

5.2.1 Thermal-hydraulic performance

To assess the real practical potential for improving the efficiency of micro-channel heat exchangers using VGs, it is important to combine the heat transfer performance with an appreciation of the fluid flow penalty resulting from the constriction of the channel. Clearly there is a huge design space available for the optimization of cylindrical VGs, however a full optimization study is beyond the scope of this paper. Instead, to illustrate the potential of such VGs, calculation of the performance evaluation criteria (PEC) index, equation (7), is made just for the VG type considered here that showed the lowest thermal resistance, i.e. the centred half-circle VG.

Fig. 13 plots the PEC index as a function of the radius of the centred half-circle VG at $Re = 200$. It is found that the best radius is $30\ \mu\text{m}$ under those conditions, with the PEC reducing to unity at about $r = 175\ \mu\text{m}$. Fig. 14 extends the data to include a wider range of Reynolds number, confirming that small-radius VGs offer good potential for improving the efficiency of micro-channels operating at low Reynolds number, with $r = 30\ \mu\text{m}$ appearing to give the best performance over the widest range of Re . Though not shown in the figure, as either the VG radius or the Reynolds number increases, eventually the increase in the pressure drop due to the constriction of the channel starts to dominate and the PEC index falls below unity, indicating that the VGs are no longer beneficial in terms of the overall efficiency.

6. Conclusions:

Vortex generators (VGs) based on cylinders with quarter-circle and half-circle cross-sections attached to the base of a microchannel have been explored as a means of enhancing the efficiency of micro-channel heat exchangers / heat sinks operating under thermal loads relevant to microelectronics cooling. The effect of the VGs was quantified in terms of the thermal resistance, pressure drop along the channel, and a combination of these forming a performance evaluation criteria (PEC) index. The results showed that:

- The cylinders with a quarter-circle cross-section were not effective in reducing the thermal resistance, except marginally so when the VG radius is relatively large and the

Reynolds number relatively small. Under these conditions the increased pressure drop dominates, making the quarter-circle VGs infeasible.

- In contrast, for the VGs with half-circle cross-section spanning the whole width of the microchannel, the thermal resistance was shown to decrease monotonically with the VG radius. However, as expected the pressure drop increased with radius as a result of the increasing constriction in the flow.
- A modification of the full-span half-circle VG to produce a shorter, centred VG showed a greater reduction in the thermal resistance, while also showing a smaller increase in the pressure drop, compared to the full-span VG. This is attributed to the gap between the ends of the VG cylinder and the side walls of the micro-channel, which allows heat transfer to continue along the whole length of the side walls, and reduces the constriction of the flow.
- Further modification to introduce a central gap in the VG negated the above benefit of the continuous centred VG, showing similar thermal resistance to the full-span VG.
- Based on the PEC index, which offsets the improvement in thermal resistance against the pressure penalty, small-radius centred VGs offer good potential for improving the efficiency of micro-channels, particularly those operating at lower Reynolds number, e.g. $Re < 600$. The maximum PEC was found for a radius of 30 μm , which may prove challenging for manufacture, but good potential is also seen for radii up to 150 μm in the cases considered here.

A full, formal optimization study has not been conducted here, but the base-mounted cylindrical vortex generators offer a wide design space for further exploration and optimization.

References

1. Li, H.-Y., et al., *Enhancing heat transfer in a plate-fin heat sink using delta winglet vortex generators*. *International Journal of Heat and Mass Transfer*, 2013. **67**(0): p. 666-677.
2. Albadr, J., S. Tayal, and M. Alasadi, *Heat transfer through heat exchanger using Al₂O₃ nanofluid at different concentrations*. *Case Studies in Thermal Engineering*, 2013. **1**(1): p. 38-44.
3. Cheraghi, M., M. Raisee, and M. Moghaddami, *Effect of cylinder proximity to the wall on channel flow heat transfer enhancement*. *Comptes Rendus Mécanique*, 2014. **342**(2): p. 63-72.
4. Dixit, T. and I. Ghosh, *Review of micro- and mini-channel heat sinks and heat exchangers for single phase fluids*. *Renewable and Sustainable Energy Reviews*, 2015. **41**(0): p. 1298-1311.
5. Mehendale, S.S., A.M. Jacobi, and R.K. Shah, *Fluid Flow and Heat Transfer at Micro- and Meso-Scales With Application to Heat Exchanger Design*. *Applied Mechanics Reviews*, 2000. **53**(7): p. 175-193.
6. Kandlikar SG, G.W., *Evolution of microchannel flow passages: thermohydraulic performance and fabrication technology*. *Proceedings of the ASME international mechanical engineering congress exposition*, 2002.
7. Tuckerman, D.B. and R.F.W. Pease, *High-performance heat sinking for VLSI*. *Electron Device Letters, IEEE*, 1981. **2**(5): p. 126-129.
8. Manca, O., S. Nardini, and D. Ricci, *A numerical study of nanofluid forced convection in ribbed channels*. *Applied Thermal Engineering*, 2012. **37**(0): p. 280-292.
9. Ahmed, M.A., et al., *Effect of corrugation profile on the thermal–hydraulic performance of corrugated channels using CuO–water nanofluid*. *Case Studies in Thermal Engineering*, 2014. **4**(0): p. 65-75.
10. Wang, C.-C. and J.-S. Liaw, *Air-side performance of herringbone wavy fin-and-tube heat exchangers under dehumidifying condition – Data with larger diameter tube*. *International Journal of Heat and Mass Transfer*, 2012. **55**(11–12): p. 3054-3060.
11. Li, L., et al., *Numerical simulation on flow and heat transfer of fin-and-tube heat exchanger with vortex generators*. *International Journal of Thermal Sciences*, 2015. **92**(0): p. 85-96.

12. Johnson, T. and P. Joubert, *The influence of vortex generators on the drag and heat transfer from a circular cylinder normal to an airstream*. *Journal of Heat Transfer*, 1969. **91**(1): p. 91-99.
13. Ebrahimi, A., E. Roohi, and S. Kheradmand, *Numerical study of liquid flow and heat transfer in rectangular microchannel with vortex generators*. *Applied Thermal Engineering*, 2015. **78**(0): p. 576-583.
14. Ahmed, H.E., H.A. Mohammed, and M.Z. Yusoff, *An overview on heat transfer augmentation using vortex generators and nanofluids: Approaches and applications*. *Renewable and Sustainable Energy Reviews*, 2012. **16**(8): p. 5951-5993.
15. Min, C., et al., *Experimental study of rectangular channel with modified rectangular vortex generators*. *International Journal of Heat and Mass Transfer*, 2010. **53**(15–16): p. 3023-3029.
16. Habchi, C., et al., *Enhancing heat transfer in vortex generator-type multifunctional heat exchangers*. *Applied Thermal Engineering*, 2012. **38**(0): p. 14-25.
17. Al-Damook, A., et al., *An experimental and computational investigation of thermal air flows through perforated pin heat sinks*. *Applied Thermal Engineering*, (0).
18. Kai-Shing, Y., et al., *On the Heat Transfer Characteristics of Heat Sinks: With and Without Vortex Generators*. *Components and Packaging Technologies*, IEEE Transactions on, 2010. **33**(2): p. 391-397.
19. Leu, J.-S., Y.-H. Wu, and J.-Y. Jang, *Heat transfer and fluid flow analysis in plate-fin and tube heat exchangers with a pair of block shape vortex generators*. *International Journal of Heat and Mass Transfer*, 2004. **47**(19–20): p. 4327-4338.
20. Wu, J.M. and W.Q. Tao, *Effect of vortex generator on heat transfer in rectangular channels*. *Applied Thermal Engineering*, 2012. **37**(0): p. 67-72.
21. Khoshvaght-Aliabadi, M., S. Zangouei, and F. Hormozi, *Performance of a plate-fin heat exchanger with vortex-generator channels: 3D-CFD simulation and experimental validation*. *International Journal of Thermal Sciences*, 2015. **88**(0): p. 180-192.
22. Li, J., et al., *Numerical study on a slit fin-and-tube heat exchanger with vortex generators*. *International Journal of Heat and Mass Transfer*, 2011. **54**(9–10): p. 1743-1751.

23. Chomdee, S. and T. Kiatsiriroat, *Enhancement of air cooling in staggered array of electronic modules by integrating delta winglet vortex generators*. *International Communications in Heat and Mass Transfer*, 2006. **33**(5): p. 618-626.
24. Liu, C., et al., *Experimental investigations on liquid flow and heat transfer in rectangular microchannel with vortex generators*. *International Journal of Heat and Mass Transfer*, 2011. **54**(13–14): p. 3069-3080.
25. Ma, J., et al., *Experimental investigations on single-phase heat transfer enhancement with longitudinal vortices in narrow rectangular channel*. *Nuclear Engineering and Design*, 2010. **240**(1): p. 92-102.
26. Xia, G.D., et al., *Effects of different geometric structures on fluid flow and heat transfer performance in microchannel heat sinks*. *International Journal of Heat and Mass Transfer*, 2015. **80**(0): p. 439-447.
27. Chen, C., et al., *A study on fluid flow and heat transfer in rectangular microchannels with various vortex generators*. *International Journal of Heat and Mass Transfer*, 2014. **69**(0): p. 203-214.
28. Mirzaee, H., et al., *HEAT TRANSFER ENHANCEMENT IN MICROCHANNELS USING AN ELASTIC VORTEX GENERATOR*. 2012. **19**(3): p. 199-211.
29. Wang, J. and Y. Zhao, *Heat and fluid flow characteristics of a rectangular channel with a small diameter circular cylinder as vortex generator*. *International Journal of Thermal Sciences*, 2015. **92**: p. 1-13.
30. Shkarah, A.J., et al., *A 3D numerical study of heat transfer in a single-phase micro-channel heat sink using graphene, aluminum and silicon as substrates*. *International Communications in Heat and Mass Transfer*, 2013. **48**(0): p. 108-115.
31. Abdollahi, A. and M. Shams, *Optimization of shape and angle of attack of winglet vortex generator in a rectangular channel for heat transfer enhancement*. *Applied Thermal Engineering*, 2015. **81**(0): p. 376-387.
32. Yu, X., et al., *Development of a plate-pin fin heat sink and its performance comparisons with a plate fin heat sink*. *Applied Thermal Engineering*, 2005. **25**(2–3): p. 173-182.
33. Gurrum, S.P., et al., *Thermal issues in next-generation integrated circuits*. *Device and Materials Reliability, IEEE Transactions on*, 2004. **4**(4): p. 709-714.
34. Yuan, W., et al., *Numerical simulation of the thermal hydraulic performance of a plate pin fin heat sink*. *Applied Thermal Engineering*, 2012. **48**(0): p. 81-88.

Table Captions

Table 1: Channel classification by Mehendale et al. [5] and Kandlikar and Grande [6].

Table 2: Dimensions of the micro-channel and VGs models.

Table 3: Code validation.

Table 4. Channel classification by Mehendale et al. [5] and Kandlikar and Grande [6].

Mehendale et al. [5].		Kandlikar and Grande [6].	
Conventional channels	$D_h > 6 \text{ mm}$	Conventional channels	$D_h > 3 \text{ mm}$
Compact Passages	$1 \text{ mm} < D_h \leq 6 \text{ mm}$	Minichannels	$1 \mu\text{m} < D_h \leq 3 \text{ mm}$
Meso-channels	$100 \text{ mm} < D_h \leq 1 \text{ mm}$	Microchannels	$10 \mu\text{m} < D_h \leq 200 \mu\text{m}$
Micro-channels	$1 \mu\text{m} < D_h \leq 100 \mu\text{m}$	Transitional channels	$0.1 \mu\text{m} < D_h \leq 10 \mu\text{m}$
		Molecular nanochannels	$D_h \leq 0.1 \mu\text{m}$

Table 5: **Dimensions of the micro-channel and VGs models.**




Micro- channel dimensions, μm					
L	25000	H_t	900	H_c	700
W_w	300	W_c	500	x_{in}	4000
VGs dimensions μm					
Models	Dimensions		Front view of the geometry		
full-span	500				
centred	300				
split	300 overall, gap 50-100				

Table 6: Code validation

Angle of VG	45°	45°
Re	233	350
Heat flux	1 kW/m^2	1 kW/m^2
T (K) present	307	305
T (K) [31]	306.362	305.617

Figure captions

Figure 1: Geometry description: (a) rectangular micro-channel containing vortex generators; (b) top view of a heat sink comprised of a series of micro-channels; (c) side-view cross-section of a quarter-circle vortex generator; (d) side-view cross-section of a half-circle vortex generator; (e) view along the channel showing the definition of parameters governing the dimensions of the geometry; (f) boundary conditions applied.

Figure 2: Grid independence test for a smooth channel, showing the maximum temperature calculated using increasingly refined meshes, with $q = 100 \text{ W/cm}^2$ and $Re = 600$.

Figure 3: Grid independence test for micro-channel with VGs; $q = 100 \text{ W/cm}^2$, $Re = 600$.

Figure 4: Code validation by comparison of calculated temperature distribution along a graphene micro-channel with heat flux 181 W/cm^2 and flow rate $8.6 \text{ cm}^3/\text{s}$ [30].

Figure 5: Code validation by comparison of calculated temperature distribution along a graphene micro-channel with heat flux 277 W/cm^2 and flow rate $8.6 \text{ cm}^3/\text{s}$ [30].

Figure 6: Thermal resistance and pressure drop as a function of Reynolds number for a micro-channel including half-circle VGs.

Figure 7: Thermal resistance and pressure drop for full-span quarter-circle VGs as a function of radius at low Reynolds number.

Figure 8: Effect of using split quarter-circle VGs: (a) thermal resistance and pressure drop at high Reynolds number; (b) temperature contours at $Re = 1100$.

Figure 9: Thermal resistance and pressure drop as a function of VG radius for full-span half-circle VGs: (a) $Re = 100$ to 900 ; (b) $Re = 1100$ to 1500 .

Figure 10: Thermal resistance and pressure drop as a function of VG radius for 'centred' half-circle VGs: (a) $Re = 100$ to 900 ; (b) $Re = 1100$ to 2300 .

Figure 11: Thermal resistance and pressure drop as a function of VG radius for split half-circle VGs: (a) $Re = 100$ to 900 ; (b) $Re = 1100$ to 2300 .

Figure 12: Comparison of the thermal resistance and pressure drop characteristics of all variants of half-circle VG considered, with radius equal to $200 \mu\text{m}$.

Figure 13: Performance evaluation criteria index determined for the centred half-circle VGs with different radii and $Re = 200$.

Figure 14: Variation of PEC index with Reynolds number for centred half-circle VGs of various radii.

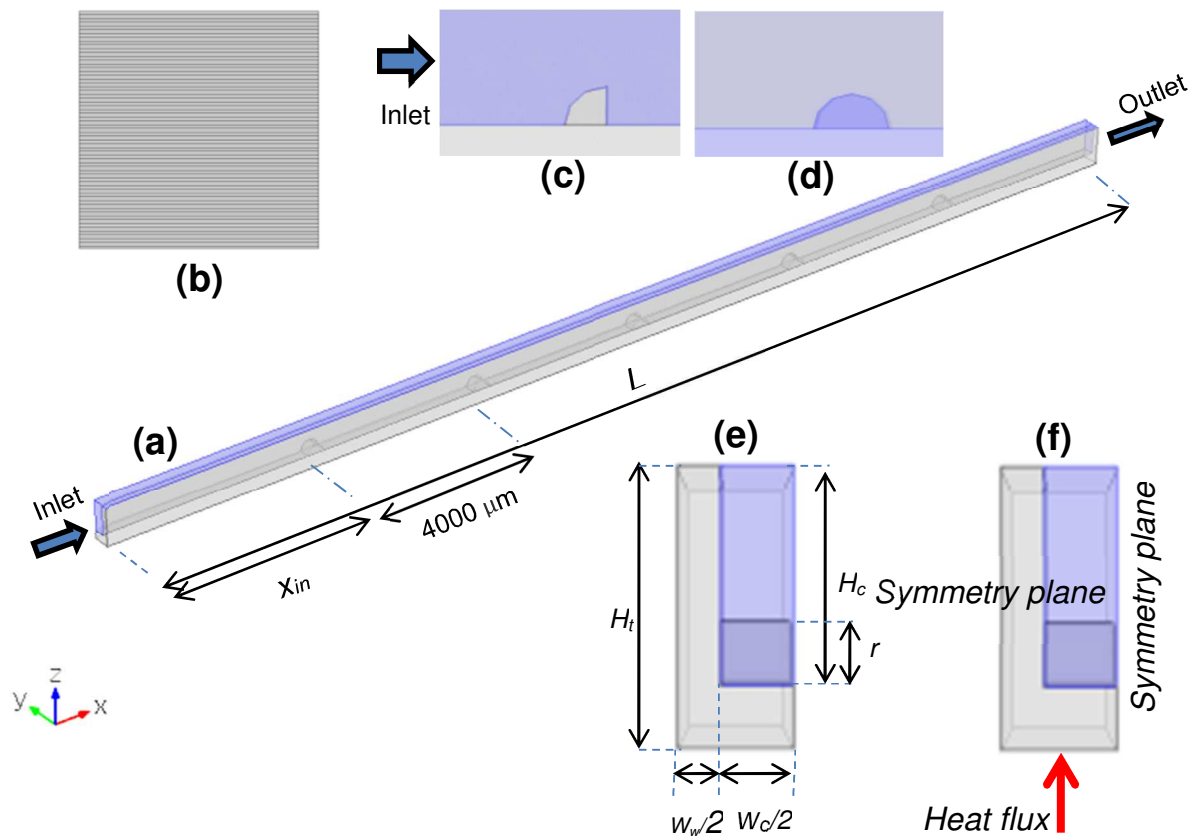


Figure 1: Geometry description: (a) rectangular micro-channel containing vortex generators; (b) top view of a heat sink comprised of a series of micro-channels; (c) side-view cross-section of a quarter-circle vortex generator; (d) side-view cross-section of a half-circle vortex generator; (e) view along the channel showing the definition of parameters governing the dimensions of the geometry; (f) boundary conditions applied.

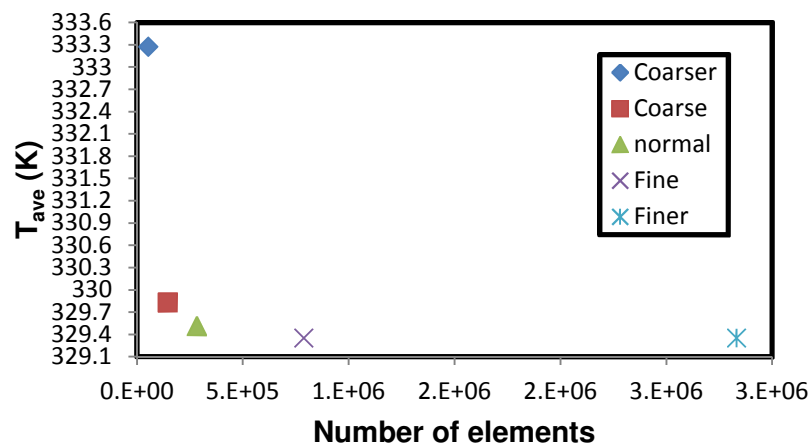


Figure 2: Grid independence test for a smooth channel, showing the maximum temperature calculated using increasingly refined meshes, with $q = 100 \text{ W/cm}^2$ and $Re = 600$.

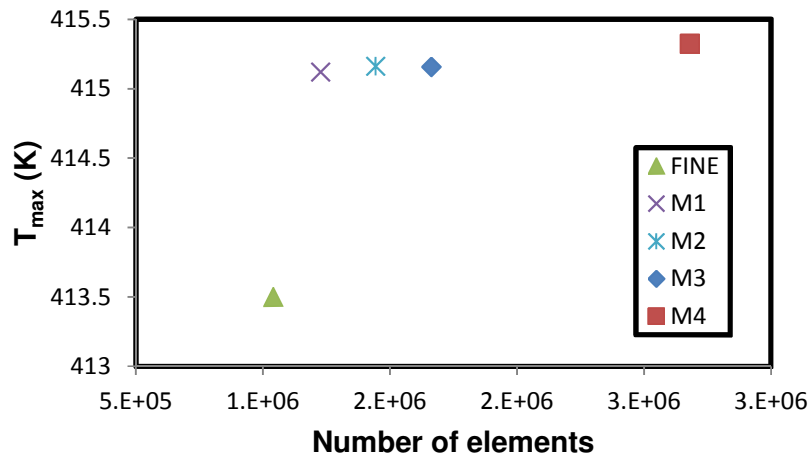


Figure 3: Grid independence test for micro-channel with VGs; $q = 100 \text{ W/cm}^2$, $Re = 600$.

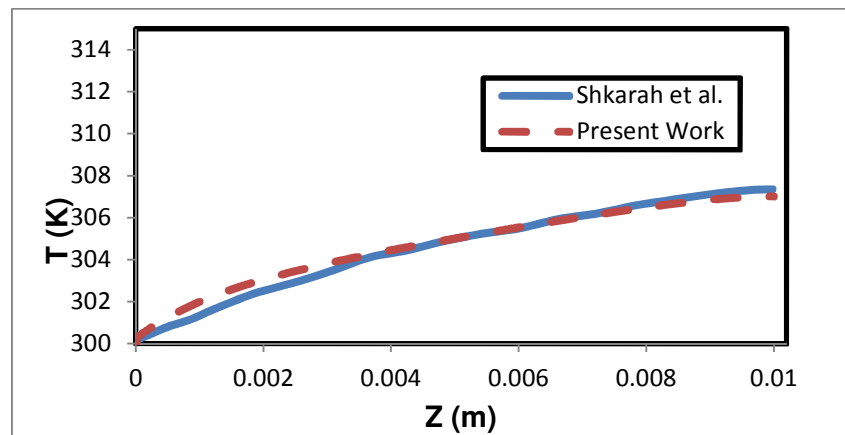


Figure 4: Code validation by comparison of calculated temperature distribution along a graphene micro-channel with heat flux 181 W/cm^2 and flow rate $8.6 \text{ cm}^3/\text{s}$ [30].

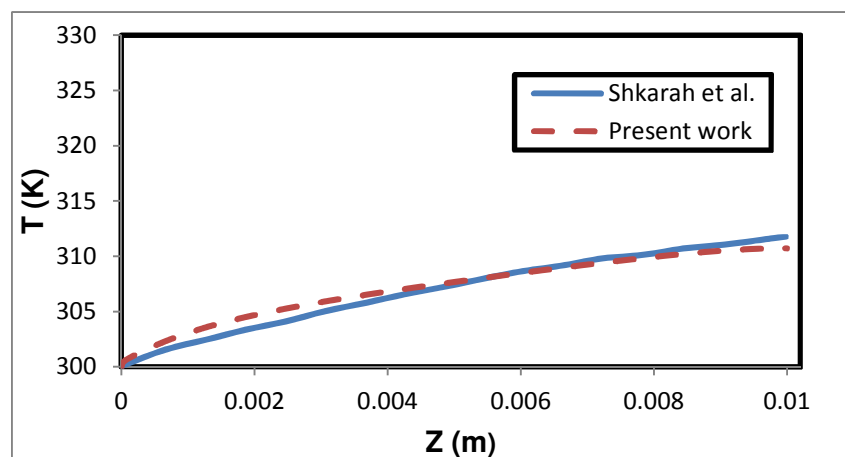


Figure 5: Code validation by comparison of calculated temperature distribution along a graphene micro-channel with heat flux 277 W/cm^2 and flow rate $8.6 \text{ cm}^3/\text{s}$ [30].

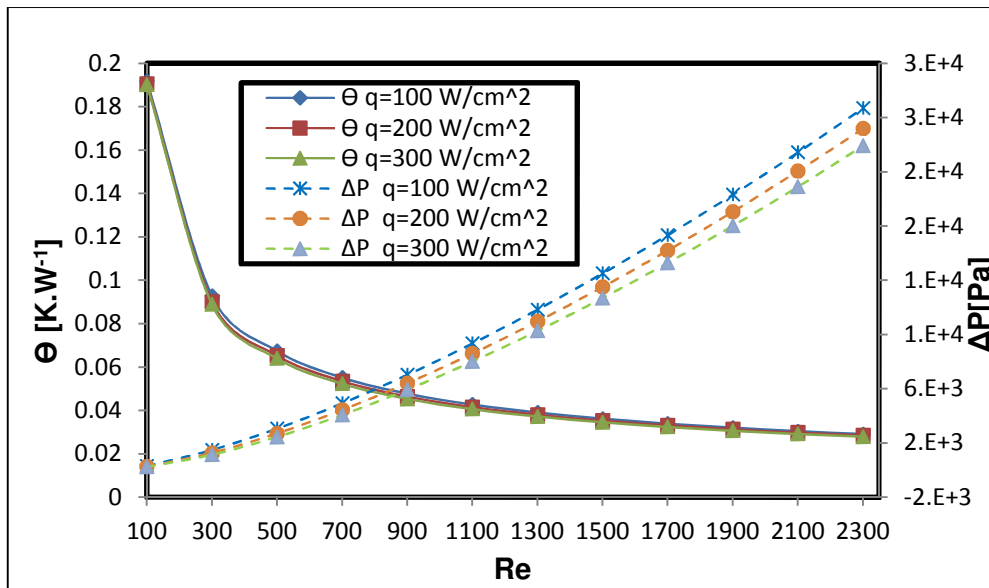


Figure 6: Thermal resistance and pressure drop as a function of Reynolds number for a micro-channel including half-circle VGs.

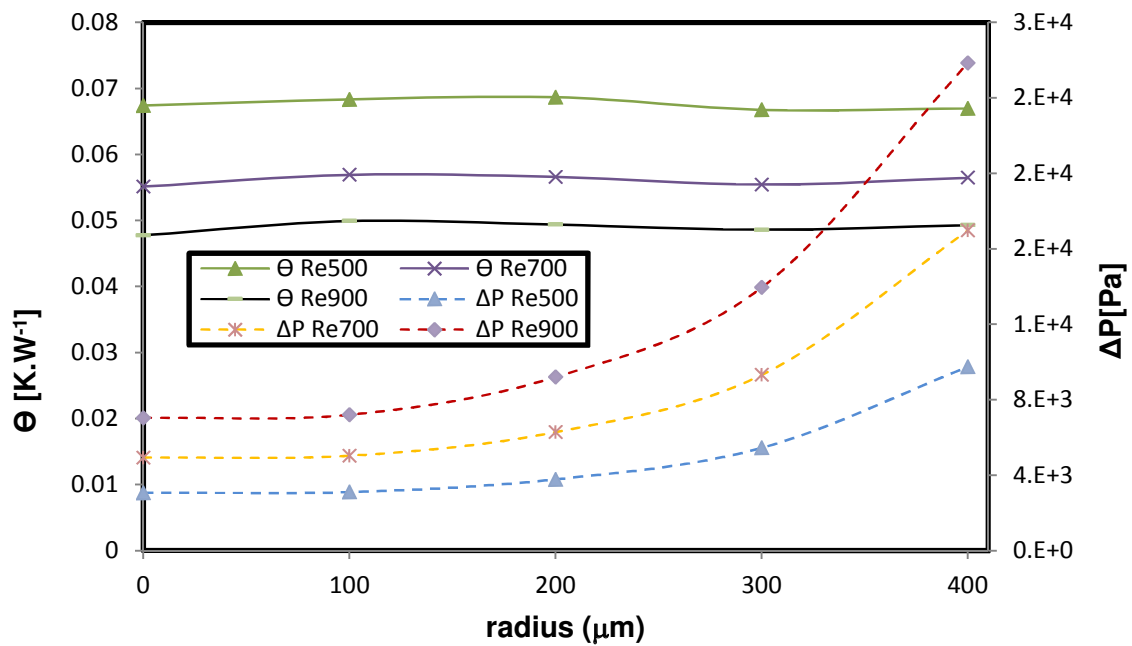


Figure 7: Thermal resistance and pressure drop for full-span quarter-circle VGs as a function of radius at low Reynolds number.

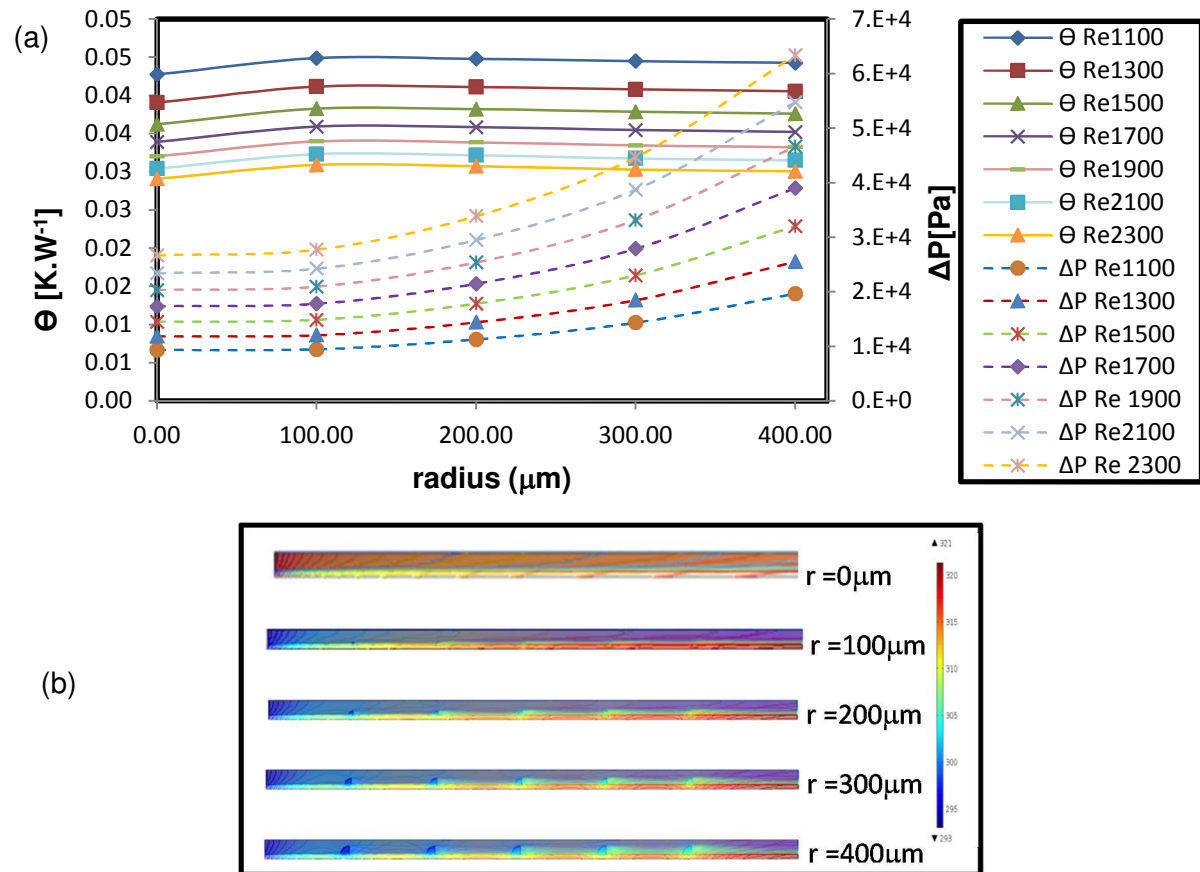


Figure 8: Effect of using split quarter-circle VGs: (a) thermal resistance and pressure drop at high Reynolds number; (b) temperature contours at $\text{Re} = 1100$.

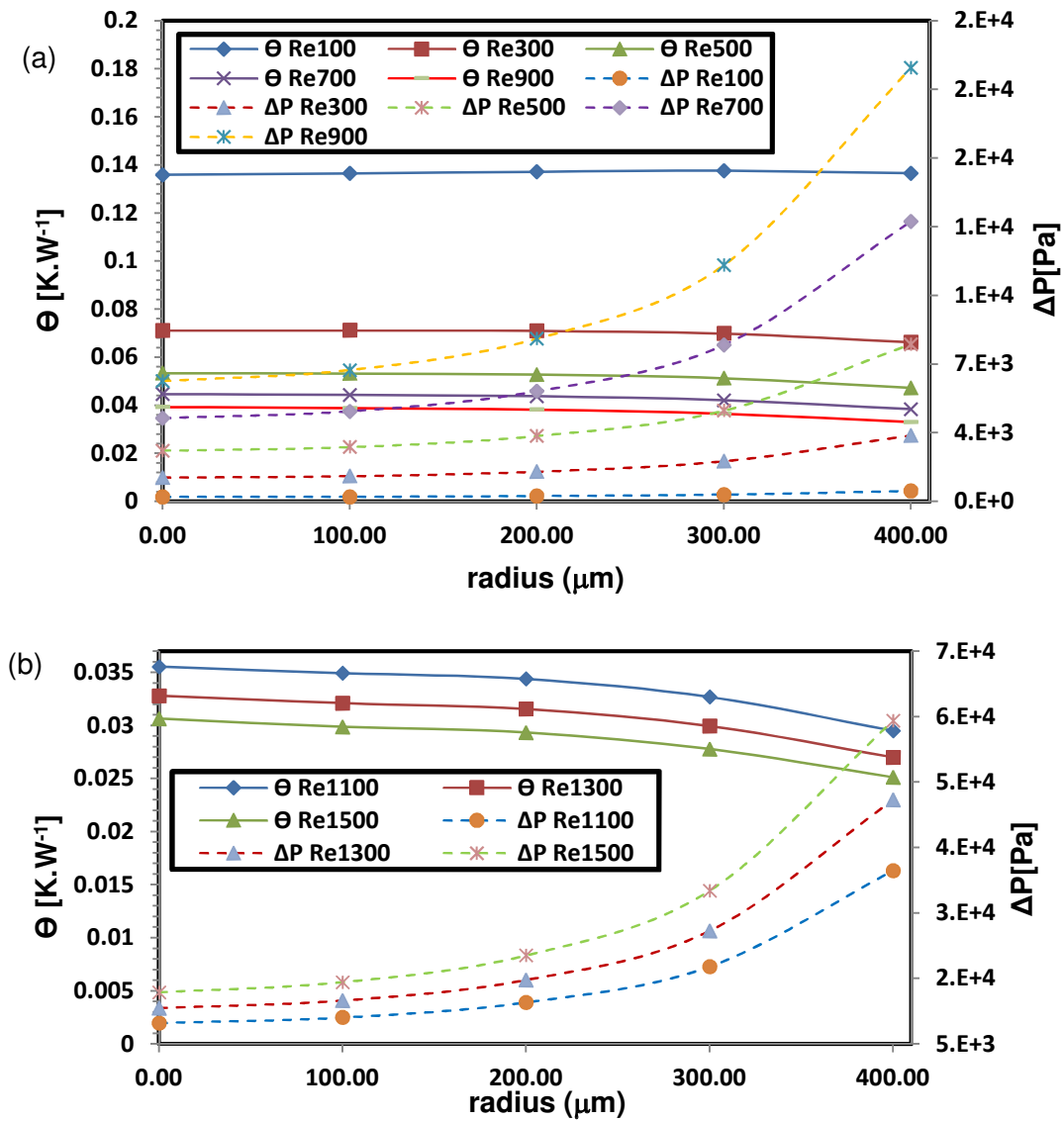


Figure 9: Thermal resistance and pressure drop as a function of VG radius for full-span half-circle VGs: (a) Re = 100 to 900; (b) Re = 1100 to 1500.

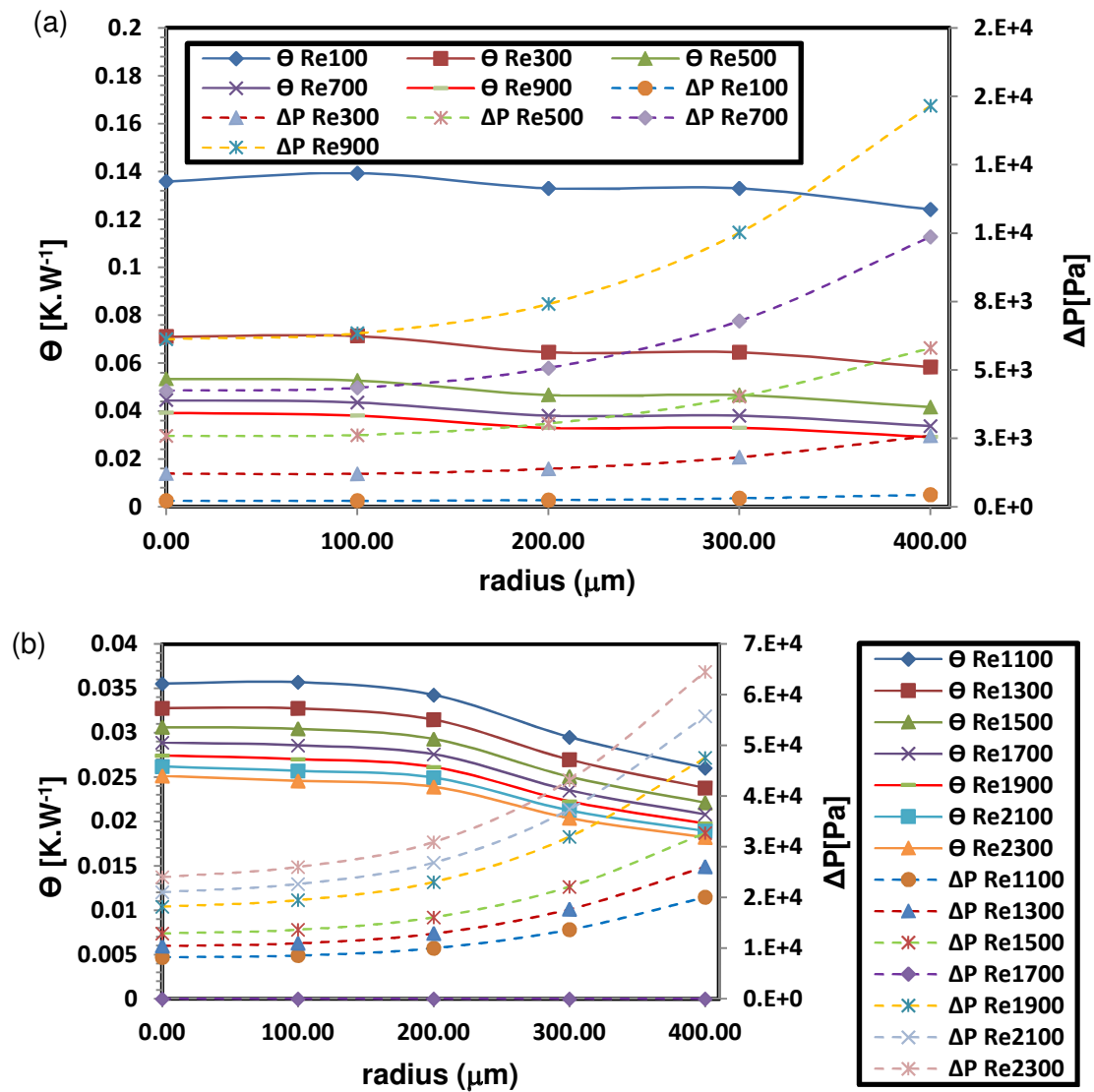


Figure 10: Thermal resistance and pressure drop as a function of VG radius for 'centred' half-circle VGs: (a) Re = 100 to 900; (b) Re = 1100 to 2300.

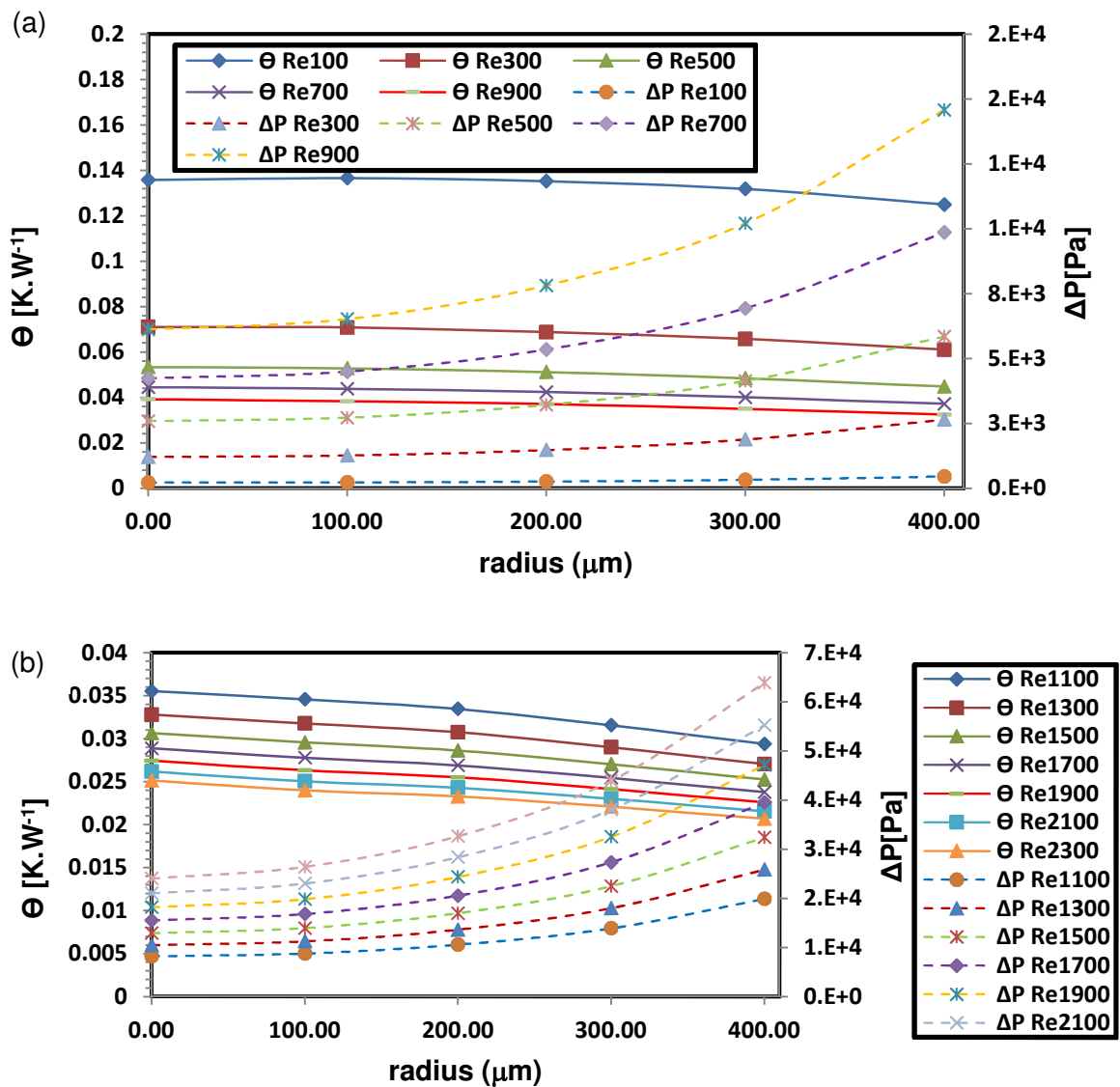


Figure 11: Thermal resistance and pressure drop as a function of VG radius for split half-circle VGS: (a) Re = 100 to 900; (b) Re = 1100 to 2300.

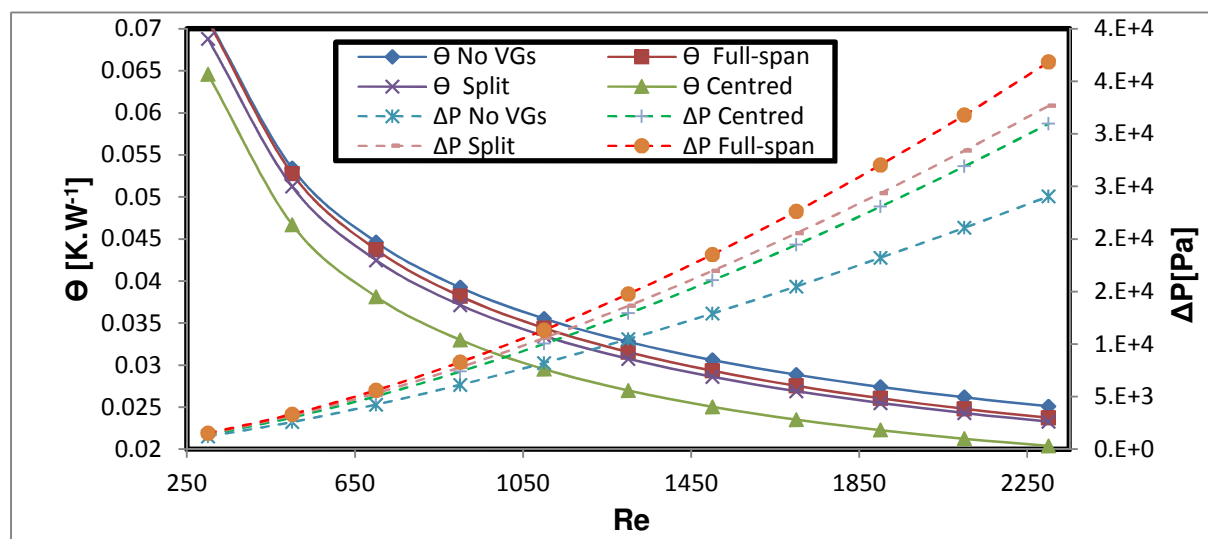


Figure 12: Comparison of the thermal resistance and pressure drop characteristics of all variants of half-circle VG considered, with radius equal to 200 μm .

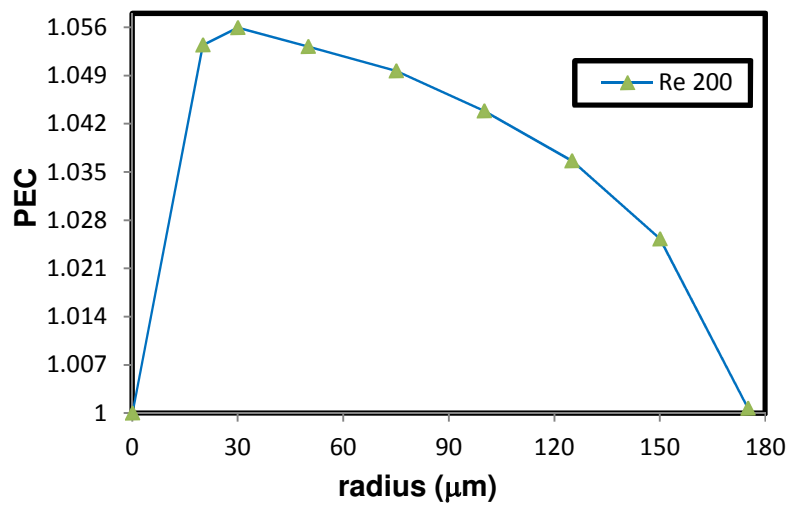


Figure 13: Performance evaluation criteria index determined for the centred half-circle VGs with different radii and $\text{Re} = 200$.

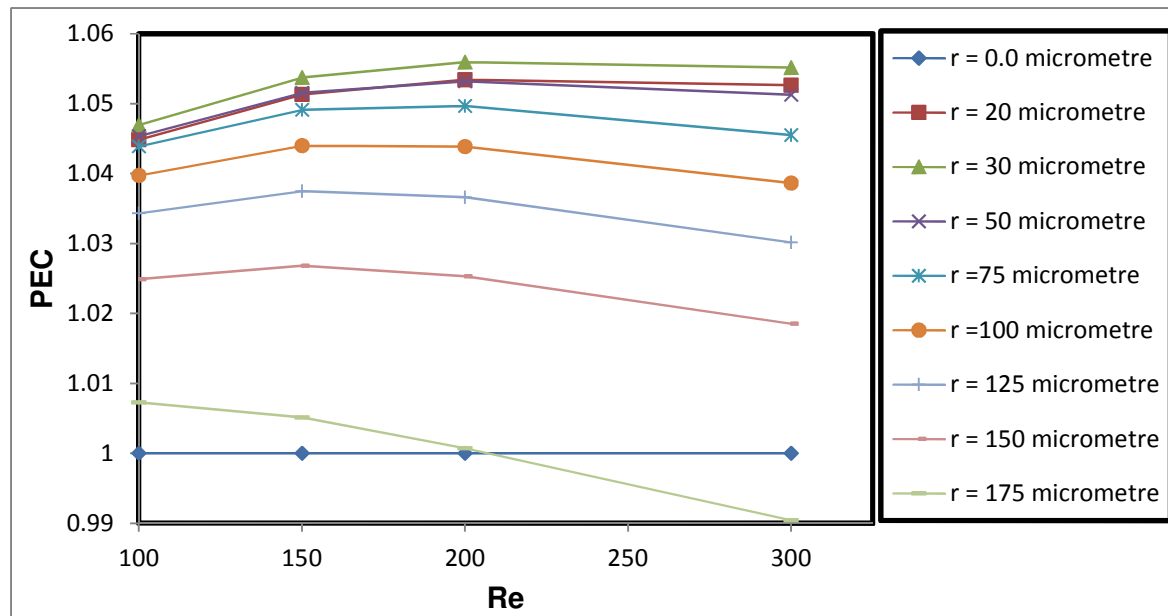


Figure 14: Variation of PEC index with Reynolds number for centred half-circle VGs of various radii.